Near-field Second Harmonic Imaging of Granular Membrane Structures in Natural Killer Cells

Richard D. Schaller,[†] Claude Roth,[‡] David H. Raulet,[‡] and Richard J. Saykally*,[†]

Department of Chemistry, University of California, Berkeley, CA, 94720 and Department of Molecular and Cellular Biology, University of California, Berkeley, CA, 94720

Received: January 24, 2000; In Final Form: March 15, 2000

Second Harmonic Generation (SHG) has been used in combination with a near-field scanning optical microscope (NSOM) to image biological samples for the first time. Near-field SHG images of azure B stained mouse natural killer (NK) cells were recorded at four different wavelengths using a tunable near-infrared femtosecond laser. The surface specificity of SHG allows membrane structures to be selectively imaged with subdiffraction spatial resolution under ambient conditions. Resonance enhancement of SHG is shown to provide a chemically specific contrast mechanism in NSOM imaging, revealing submicron features associated with the cytolytic granular membrane.

Introduction

Natural killer cells are a class of white blood cells that attack pathogen-infected cells.[1] The mechanism by which both NK and cytotoxic T cells recognize target cells and mediate cell killing is of much current interest.[2−6] Membrane-bound cytolytic granules that contain perforins and granzymes are found in both cell types. Upon binding of a target cell, the granules fuse directionally with the NK cell membrane, releasing the contents toward the target cell. Relatively little is known about the dynamics of granule release, and the ability to optically image granular membrane structures within NK cells would clearly facilitate efforts to characterize this process.[7,8] Conventional or confocal optical microscopy techniques produce an image averaged over the depth of field and thus cannot accomplish this.

SHG is a well-established optical technique for studying materials with very high surface/interface specificity and has been used in a wide variety of applications.[9−12] The magnitude of the second harmonic polarization, $P^{(2)}$, (eq 1)

$$P_i^{(2)}(2\omega) = \chi_{ijk}^{(2)} E_j(\omega) E_k(\omega) \quad (1)$$

induced in a sample is proportional to the elements of a nonlinear susceptibility tensor, $\chi_{ijk}^{(2)}$, and the square of the electric field, E, produced by an excitation pulse at the fundamental frequency ω, where i, j, and k are laboratory coordinates. In the dipole approximation, only materials that lack an inversion center can have a nonzero $\chi^{(2)}$, which necessarily includes all interfaces (e.g., membranes). SHG is also sensitive to molecular symmetry, orientation and can be detected with even submonolayer amounts of sample.[13] $\chi^{(2)}$ can be decomposed into the sum of resonant and nonresonant parts. When either ω or 2ω approaches the resonant frequency of a molecular transition (electronic, vibrational, rotational, etc.) the number of 2ω photons produced can increase by up to 10^4.[13] This resonant enhancement, because it is *chemically specific*, is appealing as a selective contrast mechanism in biological imaging. Moreover, as the IR and/or UV−Vis spectral absorptions can be used to excite distinct chemical environments in a sample one could eliminate the need to attach external chromophores (dyes), as recently demonstrated in linear (bulk-probing) near-field experiments.[14,15] Particularly, membranes and membrane-bound structures could be selectively characterized without special preparation of the sample, under ambient conditions, and perhaps even in vivo.

Near-field detected SHG experiments have recently been performed on metal surfaces,[16,17] a piezoceramic,[18] and Langmuir−Blodgett films,[19] but there have been no reports of SHG NSOM on biological materials, which are far more difficult to study because of their small values of $\chi^{(2)}$ and low optical damage thresholds. The theory of SHG NSOM has been discussed,[20] and it is proposed that the relaxation of phase-matching conditions in the near-field can actually increase the amount of 2ω photons detected relative to far-field measurements, despite an attenuation of 1 in 10^6 photons due to the use of an adiabatically pulled near-field probe that collects the SHG signal. Phase-matching relaxation also makes it possible to observe SHG signals from small sources that might otherwise not be observable in the far-field because of Mie scattering size effects.[21] Here, we describe the application of SHG NSOM for subdiffraction chemical imaging of the granular membrane structure of natural killer cells.

Experimental Section

Long-term murine cell clones were obtained from the bone marrow of P53-/-C57B1/6 mice (Taconics, USA). Briefly (C. R. and D. H. R. unpublished results), purified bone marrow precursor cells were seeded at 2 cells/well onto irradiated stromal cells in RPMI-1640 (Gibco, Grand Island, NY) supplemented with 10% fetal calf serum, 2 mM glutamine, 50 μM 2-mercaptoethanol, 10 mM HEPES and antibiotics. The resulting NK cell lines were subcloned twice at 1 cell/well in complete medium containing human rIL-2 in 96-well flat bottom plates (Falcon 3077). The clones used exhibit cytotoxicity specific for the NK-sensitive YAC-1 target cells. Giemsa (Aldrich) component stained cytospin preparations of NK cell clones were used for microscopy experiments. The unstained cells were first

[†] Department of Chemistry.
[‡] Department of Molecular and Cellular Biology.

10.1021/jp000276t CCC: $19.00
Published on Web 05/11/2000

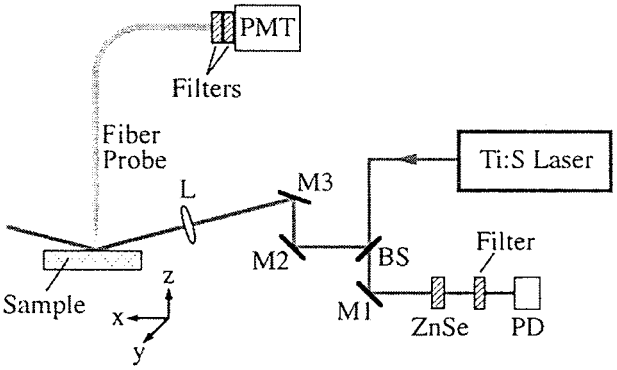

Figure 1. Experimental design of the femtosecond Chemical Imaging Ultramicroscope (CIM). Beam splitter (BS), 12 cm focal length lens (L), steering mirrors (M1−3).

allowed to air-dry on a microscope slide. The cells were then immersed in a 10^{-3} M azure B/water solution for 45 min, rinsed with distilled water, and then allowed to air-dry.

A Thermomicroscopes Lumina NSOM system, equipped with a shear-force, tuning fork, feedback system was employed for the near-field measurements. The frequency of the tuning forks was ∼95 kHz, and the tip was dithered ∼5 nm from the sample surface. Fiber optic probes were adiabatically pulled to a ∼50 nm diameter tip and were not metal coated so as to avoid significant perturbation of the sample.[16] Topography and optical signals were obtained simultaneously for comparison. The sample was not scanned in a raster pattern, but instead, the forward and reverse motions of the sample were collected as separate images as a check of image reproducibility. Repeatable optical images were then added together to reduce random noise.

The output of a home-built titanium/sapphire oscillator operating at 800 nm (480 mW, 30 fs, 88 MHz) was used to seed a commercial (Quantronix, Titan I) chirped pulse amplifier (810 nm, 2.0 W, 80 fs, 1 kHz). The amplified pulses were made tunable in the near-infrared with a commercial (Quantronix, Topaz) superfluorescence optical parametric amplifier (OPA) (1.16−2.7 μm, 350 mW at 1350 nm, 80 fs, 1 kHz). SHG experiments were conducted at four specific incident wavelengths, 1.25, 1.30, 1.35, and 1.40 μm. The near-infrared beam was attenuated to ∼10 to 12 mW and beamsplit 50/50 into a sample and reference beam. As shown in Figure 1, the sample beam was incident on the sample at 65° from normal with vertical polarization. The light was focused to a ∼50−100 μm^2 spot, and the NSOM probe was fixed while the sample was scanned to maintain a more constant tip/field geometry. SHG signals were collected by the fiber tip, filtered, and detected using an R928 Hamamatsu photomultiplier tube (PMT) with fast gated electronics. To normalize for shot to shot peak power fluctuations, the reference beam was passed unfocused through a zinc selenide window, and the strong SHG was detected with a silicon photodiode (PD). All of the SHG scans are 200 × 200 pixel *x*, *y* arrays, and each pixel *z*-value represents the average of 40 laser shots. Each pixel represents a 50 nm^2 area, except where indicated. Typically 0−3 photons were collected per shot, and complete images required ∼35 min to collect. Photobleaching of the sample in these SHG experiments is believed to be negligible due to the repeatability of the experiment.

Linear scans were performed after all SHG images were completed so as to minimize the effect of photobleaching. The output of the OPA was frequency doubled in a BBO crystal, attenuated to ∼3 mW, and then beamsplit 50/50 into a sample and reference beam. The reference beam was incident on a photodiode for normalization of pulse energy fluctuations. All linear scan pixel *z*-values represent the average of 10 shots.

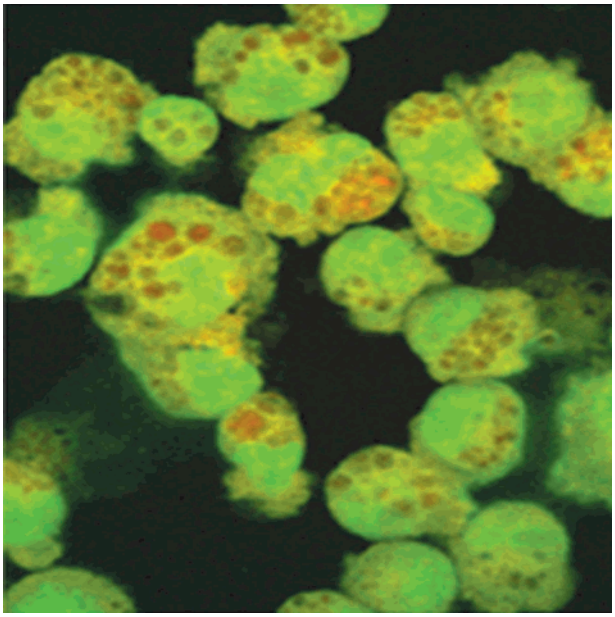

Figure 2. Confocal fluorescence microscopy image of NK cells. The image shown is a 1024 × 1024 pixel array resulting from the average of two scans, each acquired in 10 s. The fluorescence signals are shown with green indicating eosin Y fluorescence and azure B fluorescence in red. The red fluorescence is generated predominantly from small spherical features, which are localized together, indicative that azure B specifically stains the cytolytic granules. The field of view is 71 by 76 μm. Spatial resolution is approximately 600 nm. Depth of field is ∼1.2 μm.

Confocal microscope fluorescence images were collected from an eosin Y (a low specificity protein stain) and azure B stained sample of NK cells using a Zeiss 510 microscope with a 100× oil immersion lens. Five mW of 488 nm (Ar+) and 10 mW of 633 nm (HeNe) were used for excitation of the respective stains. The fluorescence signals were separated with a dichroic mirror, a band-pass filter (505−550 nm), and a long pass (>650 nm) filter and detected on separate photomultiplier tubes (PMTs) at −800 V. Pinhole sizes were 230 and 241 μm, respectively, corresponding to an optical spectral depth of ∼1.2 μm. The confocal image shown in Figure 2 is a 1024 × 1024 pixel array resulting from the average of two scans, each acquired in 10 s.

The UV−Vis spectra were acquired with a Hewlett-Packard 8453 diode-array spectrophotometer and a quartz sample cell with 1 nm spectral resolution.

Results and Discussion

Confocal fluorescence microscopy was performed on azure B stained NK cells to demonstrate the high specificity of azure B for cytolytic granules. Figure 2 shows the overlaid image of fluorescence from eosin Y (a low specificity stain) in green with the fluorescence of azure B in red. The red fluorescence is produced predominantly from small spherical features that are grouped together. These features are clearly granules that appear to be evenly and specifically stained. Although confocal microscopy represents the highest resolution available with a far-field optical microscope (ultimately limited by diffraction effects to $\lambda/2$), fluorescence probes the *bulk* of a sample and is relatively insensitive to surfaces.

Figure 3, parts **b**−**e**, shows reproducible SHG NSOM images at 2ω = 625, 650, 675, and 700 nm of the same 10 μm^2 topographic region shown in **a**, generated with the tunable near-

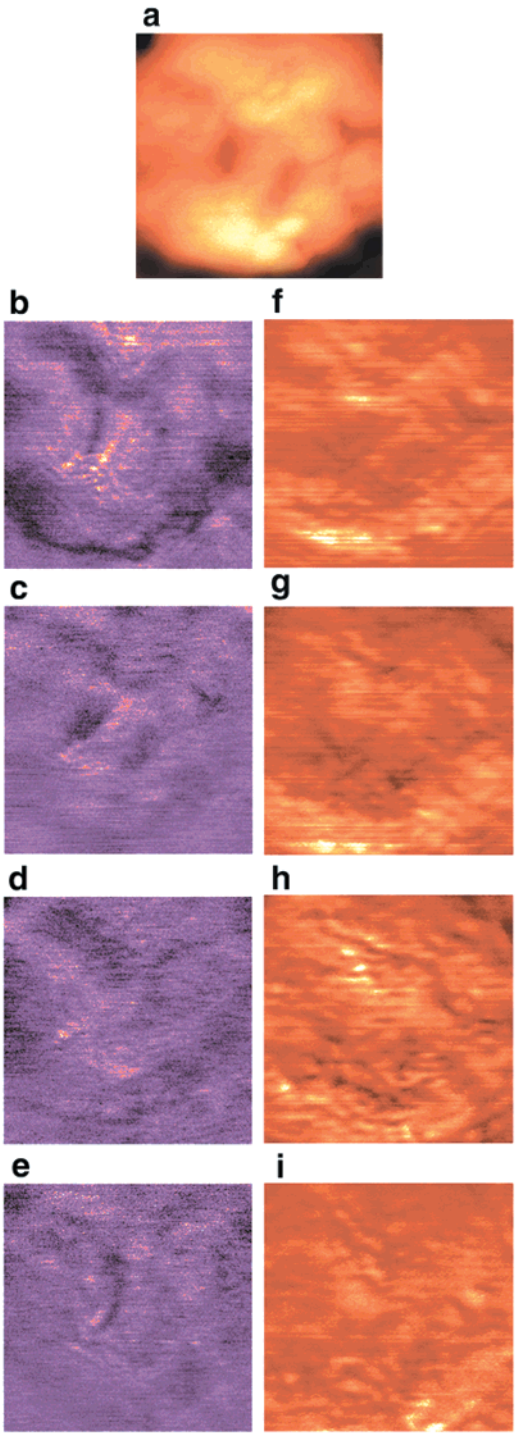

Figure 3. CIM images of an azure B stained NK cell. A Topography of an azure stained NK cell in a 10 μm^2 area; **b**−**e**, SHG NSOM images of the same area produced at 2ω = 625, 650, 675, and 700 nm, respectively; **f**−**i**, Linear NSOM reflectivity images produced at ω = 625, 650, 675, and 700 nm, respectively. SHG contrast is highest in **b** when 2ω is resonant with an azure B electronic absorption. The fact that contrast is lower at 2ω = 650 nm than at 2ω = 625 nm indicates a shift of the resonance of the azure B stain to higher frequencies and is the result of the intracellular environment of the stain. Such an effect could be produced by solvatochromism. Linear images resemble the SHG images, which indicates that second-order polarizabilities are the main source of contrast rather than the linear reflective indices. The dark outline of the NK cell in **b**, and evident to a lesser degree in all of the other SHG images, appears sharper in **b** due to the higher signal-to-noise ratio. Dark areas in SHG images correspond to low signal (~0 photons/shot), light areas correspond to high signal (~3 photons/shot). The topographic height of **a** is 1.44 μm.

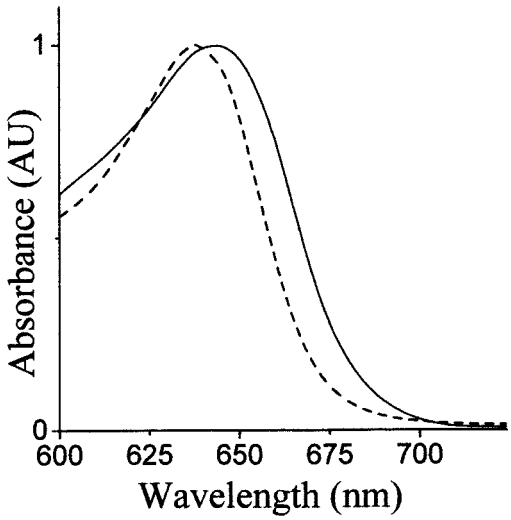

Figure 4. Solvatochromism of azure B. Comparison of visible absorption spectra of azure B in water (solid line) and also a 50/50 v/v mixture of acetone/hexanes (dashed line) show that the λ_{max} of azure B shifts from 650 nm in water to 638 nm in the lower polarity solvent mixture. Azure B and most of the related phenothiazine dyes are highly solvatochromic due to the electron-transfer nature of the excited state.[27] Electron-transfer absorption bands are sensitive to the polarity of the environment, being red shifted in high-polarity solvents and blue shifted in low-polarity solvents.[28,29] This blue shift, which may be even larger in the granular membrane, is enough to effect higher SHG NSOM contrast at 625 nm (Figure 3**b**) than at 650 nm (Figure 3**c**). In both solvent systems, azure B has negligible absorption near 700 nm, which is consistent with poor SHG contrast in Figure 3**e**. The shift in the maximum of the electron-transfer resonance of the stain may be a useful tool in measuring biological microenvironments.

infrared femtosecond laser. Of the four optical frequencies used, 2ω = 625 nm produces the highest contrast, followed by 650 nm, whereas 675 and 700 nm produce similar lower contrast images. The sharp increase in SHG contrast when 2ω is tuned to 625 nm corresponds to the strong absorption of the azure B dye molecule ($\epsilon \approx 10^4$ to 10^5) and is a result of resonant enhancement. The shift in resonance wavelength from 650 nm in pure water toward 625 nm in the NK cells is probably due to a solvatochromic shift of the azure B stain to shorter wavelength, as demonstrated in Figure 4, indicating that it is located in a very low polarity environment, viz. the granular membrane. Further work is required to confirm whether this solvatochromic shift is the only effect contributing to the observed blue-shifted resonance.[22]

Linear reflectivity NSOM images of the same topographical region, shown in Figure 3**a** produced at 625, 650, 675, and 700 nm, are shown in Figure 3, parts **f**−**i**, respectively. The striking dissimilarity between the linear images and the SHG images shows that the spatial variation in $\chi^{(2)}$ of a sample provides a unique contrast mechanism that strongly complements the usual (linear) optical response operative in conventional microscopy.

The possibility of a signal resulting from two-photon fluorescence has been considered. Both types of signals will depend quadratically upon input intensity, however, due to the fact that the observed signal has a time decay limited by that of the PMT detector (~2 ns), the signal appears to be coherent and is, thus, highly indicative of either SHG or very fast fluorescence. The fluorescence lifetimes of azure B have not yet been reported. However, the lifetimes for azure A (which is very similar electronically and structurally to azure B) have been determined to be dominated by a triplet state relaxation which has been measured to be ~0.4 μs.[23] No such long temporal decay process was observed, and therefore, the signal is believed to be SHG.

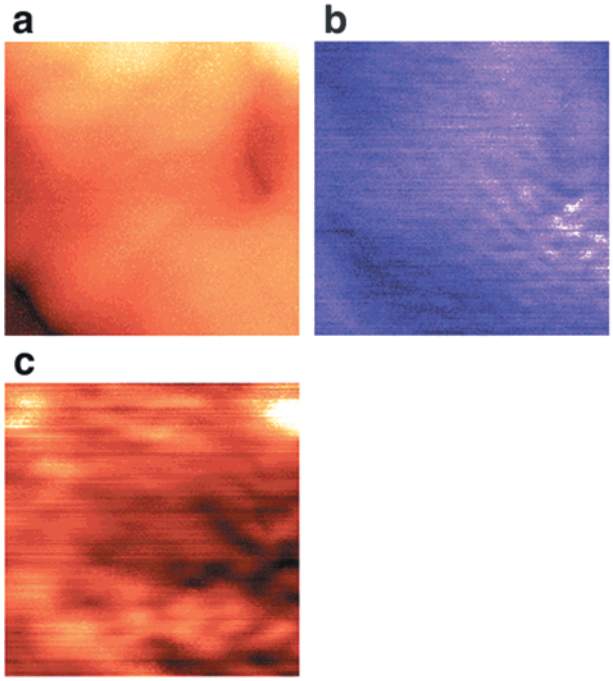

Figure 5. Zoomed view of an azure B stained NK cell. **a**, Topography; **b**, SHG at $2\omega = 625$ nm; and **c**, linear reflectivity at $\omega = 625$ nm of the 5 μm^2 area corresponding to the lower left quadrant of Figure 3**a**. Pixel size in these images is 25 nm^2. Small repeatable round features ($\sim$300 nm fwhm) are evident in the SHG image but are clearly not present in the corresponding linear image. These small spheroids are azure B stained granules that are organized on a membrane feature of the NK cell and can be selectively imaged due to the surface selective resonantly enhanced SHG produced from the adsorbed stain.

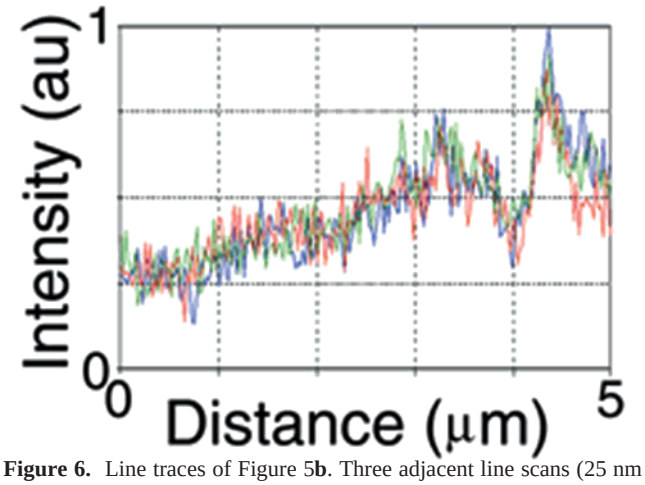

Figure 6. Line traces of Figure 5**b**. Three adjacent line scans (25 nm separation) of Figure 5**b** show the highest intensity SHG feature from the azure B stained NK cell. The highly reproducible granular feature centered at 4.4 μm shows a fwhm spatial resolution of $\sim$300 nm, which may be sample limited.

The topography, SHG at $2\omega = 625$ nm, and linear reflectivity at $\omega = 625$ nm of a 5 μm^2 area zoomed in from Figure 3 are compared in Figure 5, parts **a**−**c**, respectively. It can be seen in the SHG image that what may appear as ridges in the 10 μm^2 scans are actually small, discrete spots corresponding to granule locations, which appear bright due to the resonant enhancement from the stain. The spatial resolution, probably sample limited, is demonstrated to be $\sim$300 nm in Figure 6 at the fwhm of one of the brighter spots, significantly higher than that obtained with the confocal microscope ($\sim$600 nm).

In summary, we have presented the initial demonstration of a chemical imaging ultramicroscope based on near-field imaging of the second harmonic response of a sample. We have shown that the technique can image selected chemical environments in situ at subdiffraction spatial resolution via the resonant enhancement of the SHG, and that, unlike fluorescence microscopy, it is also highly selective for membrane (rather than bulk) structures. We describe the first application of SHG NSOM to a biological sample, imaging the cytolytic granular membrane structure of natural killer cells. Future work will seek to exploit selective chemical imaging via the vibrational modes of a sample, thereby eliminating the need for staining and making it possible to study unmodified living cells. Moreover, the ultrafast time resolution possible with femtosecond lasers can be exploited to measure dynamical processes occurring in cellular components.[24−26]

Acknowledgment. R.D.S. and R.J.S. are supported by the Experimental Physical Chemistry Division of the National Science Foundation and also acknowledge the Keck Foundation for supporting the UCB/UCLA Joint Institute for Chemical Imaging Ultramicroscopy. C.R. and D.H.R. are supported by grants from the National Institutes of Health.

References and Notes

(1) Trinchieri, G. *Adv. Immunol*. **1989**, *47*, 187.
(2) Raulet, D. H. *Curr. Opin. Immunol.* **1996**, *8*, 372.
(3) Giorda, R.; Rudert, W. A.; Vavassori, C.; Chambers, W. H.; Hiserodt, J. C.; Trucco, M. *Science* **1990**, *249*, 1298.
(4) Yano, S.; Nishioka, Y.; Nokihara, H.; Sone, S. *Cancer Res.* **1997**, *57*, 784.
(5) Kagi, D.; Ledermann, B.; Burki, K.; Zikernagel, R. M.; Hengartner, H. *Annu. Rev. Immunol.* **1996**, *14*, 207.
(6) Griffiths, G. M.; Argon, Y. *Curr. Top. Microbiol. Immunol.* **1995**, *198*, 39.
(7) Grakoui, A.; Bromley, S. K.; Sumen, C.; Davis, M. M.; Shaw, A. S.; Allen, P. M.; Dustin, M. L. *Science* **1999**, *285*, 221.
(8) Monks, C. R. F.; Freiberg, B. A.; Kupfer, H.; Sciaky, N.; Kupfer, A. *Nature* **1998**, *395*, 82.
(9) Collier, C. P.; Saykally, R. J.; Shiang, J. J.; Henrichs, S. V.; Heath, J. R. *Science* **1997**, *277*, 1978.
(10) Henrichs, S. E.; Sample, J. L.; Shiang, J. J.; Heath, J. R.; Collier, C. P.; Saykally, R. J. *J. Phys. Chem. B* **1999**, *103*, 3524.
(11) Rasing, T.; Hung, J.; Lewis, A.; Stehlin, T.; Shen, Y. R. *Phys. Rev. A* **1989**, *40*, 1684.
(12) Lewis, A.; Khatchatouriants, A.; Treinin, M.; Chen, Z. P.; Peleg, G.; Friedman, N.; Bouevitch, O.; Rothman, Z.; Loew, L.; Sheres, M. *Chem. Phys.* **1999**, *245*, 133.
(13) Shen, Y. R. *Nature* **1989**, *337*, 519.
(14) Knoll,B.; Keilmann, F. *Nature* **1999**, *399*, 134.
(15) Dragnea, B.; Preusser, J.; Schade, W.; Leone, S. R.; Hinsberg, W. D. *J. Appl. Phys.* **1999**, *86*, 2795.
(16) Smolyaninov, I. I.; Zayats, A. V.; Davis, C. C. *Phys. Rev. B* **1997**, *56*, 9290.
(17) Smolyaninov, I. I.; Zayats, A. V.; Davis, C. C. *Opt. Lett*. **1997**, *22*, 1592.
(18) Smolyaninov, I. I.; Lee, C. H.; Davis, C. C. *Appl. Phys. Lett*. **1999**, *74*, 1942.
(19) Bozhevolnyi, S. I.; Geisler, T. *J. Opt. Soc. Am. A* **1998**, *15*, 2156.
(20) Vigoureux, J. M.; Girard, C.; Depasse, F. *J. Mod. Opt.* **1994**, *41*, 49.
(21) Kasparian, J.; Kramer, B.; Leisner, T.; Rairoux, P.; Boutou, V.; Vezin, B.; Wolf, J. P. *J. Opt. Soc. Am. B* **1998**, *15*, 1918.
(22) Xu, C.; Webb, W. W. *J. Opt. Soc. Am. B* **1996**, *13*, 481.
(23) Cheville, R. A.; Averitt, R. D.; Halas, N. J. *Opt. Comm.* **1994**, *110*, 327.
(24) Douhal, A.; Kim, S. K.; Zewail, A. H. *Nature* **1995**, *378*, 260.
(25) Greenfield, S. R.; Seibert, M.; Govindjee; Wasielewski, M. R. *J. Phys. Chem. B* **1997**, *101*, 2251.
(26) Hilgemann, D. W. *Science* **1994**, *263*, 1429.
(27) Parkanyi, C.; Boniface, C.; Aaron, J. J.; Maafi, M. *Spectrochim. Acta* **1993**, *49A*, 1715.
(28) Mes, G. F.; de Jong, B.; van Ramesdonk, H. J.; Verhoeven, J. W.; Warman, J. M.; de Haas, M. P.; Horsman-van den Dool, L. E. W. *J. Am. Chem. Soc*. **1984**, *106*, 6524.
(29) Reta, M. R.; Cattana, R.; Anunziata, J. D.; Silber, J. J. *Spectrochim. Acta* **1993**, *49A*, 903.